Accepted: 16 August 2017

DOI: 10.1111/clr.13074

ORIGINAL ARTICLE

WILEY CLINICAL ORAL IMPLANTS RESEARCH

New bone formation and trabecular bone microarchitecture of highly porous tantalum compared to titanium implant threads: A pilot canine study

Jin Whan Lee[1] | Hai Bo Wen[1] | Prabhu Gubbi[1] | Georgios E. Romanos[2]

[1]Zimmer Biomet, Palm Beach Gardens, FL, USA

[2]School of Dental Medicine, Stony Brook University, Stony Brook, NY, USA

Correspondence
Georgios Romanos, Stony Brook University, School of Dental Medicine, Stony Brook, NY, USA.
Email: georgios.romanos@stonybrook.edu

[The copyright line for this article was changed on 28 July 2018 after original online publication.]

Abstract

Aim: This study evaluated new bone formation activities and trabecular bone microarchitecture within the highly porous region of Trabecular Metal™ Dental Implants (TM) and between the threads of Tapered Screw-Vent® Dental Implants (TSV) in fresh canine extraction sockets.

Materials and methods: Eight partially edentulated dogs received four implants (4.1 mmD × 13 mmL) bilaterally in mandibular fresh extraction sockets (32 TM, 32 TSV implants), and allowed to heal for 2, 4, 8, and 12 weeks. Calcein was administered to label mineralizing bone at 11 and 4 days before euthanasia for dogs undergoing all four healing periods. Biopsies taken at each time interval were examined histologically. Histomorphometric assay was conducted for 64 unstained and 64 stained slides at the region of interest (ROI) (6 mm long × 0.35 mm deep) in the midsections of the implants. Topographical and chemical analyses were also performed.

Results: Histomorphometry revealed significantly more new bone in the TM than in the TSV implants at each healing time (p = .0014, .0084, .0218, and .0251). Calcein-labeled data showed more newly mineralized bone in the TM group than in the TSV group at 2, 8, and 12 weeks (p = .045, .028, .002, respectively) but not at 4 weeks (p = .081). Histologically TM implants exhibited more bone growth and dominant new immature woven bone at an earlier time point than TSV implants. The parameters representing trabecular bone microarchitecture corroborated faster new bone formation in the TM implants when compared to the TSV implants. TM exhibited an irregular faceted topography compared to a relatively uniform microtextured surface for TSV. Chemical analysis showed peaks associated with each implant's composition material, and TSV also showed peaks reflecting the elements of the calcium phosphate blasting media.

Conclusions and clinical implications: Results suggest that the healing pathway associated with the highly porous midsection of TM dental implant could enable faster and stronger secondary implant stability than conventional osseointegration alone; however, prospective clinical studies are needed to confirm these potential benefits in patients with low bone density, compromised healing, or prior implant failure.

KEYWORDS

dental implant, osseoincorporation, osseointegration, trabecular metal

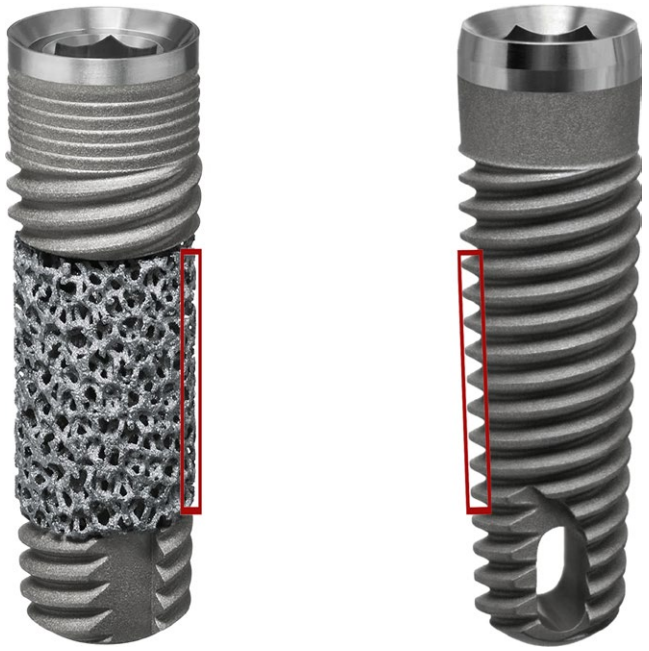

FIGURE 1 Study implants with midsections of unthreaded, highly porous TM (left) or conventional V-shaped external threads (right). Boxes (6.0 mm × 0.35 mm) indicate the regions of interest in this study

1 | INTRODUCTION

There have been many efforts to improve dental implant performance at the bone–implant interface by modifying the topography and chemistry of the implant surface (Lavenus, Louarn & Layrolle, 2010; Stanford, 2008). Another approach has been to alter the structure of the implant surface through the construction of porosity (Bencharit et al., 2014; Liu, Bao, Wismeijer, Hosseini & Wu, 2015; Pilliar, 1998). Porous surface coatings fabricated by sintering titanium beads onto titanium alloy substrates have resulted in micropores that range from 100 to 400 μm in size with ~35% porosity (Pilliar, Cameron, Binnington, Szivek & Macnab, 1979). Histologic findings of an 18-month trial in dogs showed higher bone-in-contact in the porous titanium bead implant than in a cylindrical, threaded implant (Deporter, Watson, Pilliar, Chipman & Valiquette, 1990; Pilliar, 1998).

Many studies since the 1970s have reported that the size of the pores and overall percentage of porosity are the determining factors for successful bone ingrowth (Schlee et al., 2014). While 100 μm pores have been reported as acceptable for bone ingrowth, other researchers have maintained that 150 μm pores would be needed for osteon formation and 300 μm pores would be more ideal to support the ingrowth of both bone and vascular structures inside the material (Schlee et al., 2014). Porous surface coatings have achieved some of these characteristics to varying degrees (Deporter et al., 1990), but tend to offer limited porosity with pores in irregular dimensions (Schlee et al., 2014).

Bobyn, Stackpool et al., (1999) developed a tantalum (Ta)-based, trabecular-structured biomaterial with ~80% porosity by coating a vitreous carbon scaffold with elemental Ta through a chemical vapor deposition (CVD) process (Trabecular Metal™ Material, Zimmer Biomet TMT, Parsippany, NJ, USA) (TM). The porous TM biomaterial contains a network of pores (~440 μm in size) that interconnect to form large internal dodecahedron-shaped healing chambers or cells in regular sizes and shapes (Balla, Bodhak, Bose & Bandyopadhyay, 2010; Shimko, Shimko, Sander, Dickson & Nauman, 2005; Zardiackas et al., 2001). Histologic assays of the bone ingrowth responses to the TM biomaterial in a dog model have indicated a propensity for rapid infiltration of bone tissue over healing (Bobyn, Toh et al., 1999). For dental applications, this TM biomaterial has been positioned in the midsection of a conventional titanium alloy implant body (Trabecular Metal™ Dental Implants, Zimmer Biomet, Palm Beach Gardens, FL, USA) that comprises the coronal, apical, and internal regions of the implant (Kim et al., 2013). This design has enabled TM dental implants to undergo two different healing pathways. The first healing pathway is conventional osseointegration (or bone ongrowth), which occurs at the textured tantalum and titanium implant surfaces (Kim et al., 2013; Liu et al., 2015). The second pathway is intramembranous-like healing characterized by rapid bone, blood vessel, and marrow formation inside the pores (or bone ingrowth) and internal healing chambers of the TM biomaterial (Lee et al., 2015; Smith et al., 2014). In addition to osteoconduction that occurs along the peripheral pores of the implant, preosteoblasts present in the blood clot inside the TM biomaterial have been theorized to differentiate into osteoblasts that lay down seams of osteoid, which combines with calcium to form calcified bone tissue inside the TM pores and internal healing chambers (Spinato, Zaffe, Felice, Checchi & Wang, 2014). Bencharit et al. (2014) termed this combined bone ongrowth and ingrowth healing process as "Osseoincorporation."

In a pilot dog study, Kim et al. (2013) evaluated early bone response and anchorage of TM and conventionally threaded dental implants during 12 weeks of healing in healed extraction sites and found comparable results between the two implant designs. More recently, the present authors reported (Lee et al., 2015) that TM dental implants demonstrated increased biological stability in the fresh extraction sockets of dogs as compared to conventionally threaded implants during early healing. However, further research was needed to explain this observed difference between the two implant designs. A follow-up study was conducted in fresh canine extraction sockets to evaluate new bone formation activities and the resulting trabecular bone microarchitecture inside the pores and healing chambers of TM dental implants and between the threads of conventional dental implants.

2 | MATERIALS AND METHODS

The study protocol was approved by the Animal Welfare Committee of MPI Research (Mattawan, MI) and strictly complied with domestic and international guidelines for the humane treatment of research animals. Eight healthy, one-year-old male hound dogs ranging from 15.5 to 32.5 kg in weight were selected for this study. The dogs were

allowed to acclimate to the facility for 2 weeks before they were randomly assigned to surgery.

2.1 | Study implants

The two study implants were slightly tapered designs, 4.1 mm in diameter by 13 mm in length, with microtextured (MTX® Surface, Zimmer Biomet, Palm Beach Gardens, FL, USA) titanium alloy surfaces created by grit-blasting the implants with hydroxyapatite (HA) particles, but differed in their midsections and cervical collar designs. The region of interest (ROI) in this study was the midsection of the implant, which consisted of either highly porous TM (Trabecular Metal Dental Implants, Zimmer Biomet) or conventional "V-shaped" external threads (Tapered Screw-Vent® Dental Implants, Zimmer Biomet) (Figure 1).

2.2 | Surgical procedures

Surgical procedures were performed using general anesthesia induced with sodium pentothal (14 mg/ml) intravenously. Buccal and lingual intrasulcular incisions were made and extended along the alveolar crest to include two mandibular posterior premolars (P3, P4) and both molars (M1, M2). Terminal vertical releasing incisions were made in the interdental regions posterior to the second premolar (P2) and in the retromolar regions slightly beyond the second M2 sulcus, respectively. Full-thickness buccal and lingual flaps were elevated to expose the alveolar ridge, and teeth (P3, P4, M1, M2) were extracted using an atraumatic technique in an attempt to preserve the alveolar sulci. The same procedures were performed in the contralateral quadrant of each animal. The extraction sites were prepared for immediate implant placement by sequential cutting with internally irrigated drills in graduated diameters, and four implants (two TM, two TSV) were randomly placed bilaterally in both posterior mandibular quadrants of each dog according to the manufacturer's instructions for use. The fixture mounts were removed, and surgical cover screws were attached to the tops of the implants for a submerged healing protocol.

After placement, voids around the implants were packed with bone allograft material (Puros® Cancellous Particulate Allograft, Zimmer Biomet) rehydrated in sterile saline, per manufacturer instructions, and a collagen barrier membrane (BioMend® Extend™, Zimmer Biomet) was placed over the implant and graft material. The gingival flaps were repositioned and sutured (4-0 Vicryl®, Ethicon Inc., Langhorne, PA, USA) in place using an interrupted technique while taking care to avoid tension over the exposed barrier membranes. All animals were placed on a soft diet and received mouthwashes with 0.12% chlorhexidine followed by sterile saline for at least 1 week after extraction and implantation surgery until soft tissue closure. Additional rinses were performed as needed per veterinary consultation.

2.3 | Calcein bone labeling

Each dog was injected with calcein (10 mg/kg) (Sigma Chemical Co., St. Louis, MO, USA) at 11 and 4 days before euthanasia. Calcein-bound calcium ions can produce calcium deposition by chelation (Sun, Mori, Roper, Brown & Burr, 1992) and, when viewed over time, can visually depict the dynamics of mineralized bone tissue formation (Roldan et al., 2004).

2.4 | Histologic examination

Two dogs were humanely euthanized at weeks 2, 4, 8, and 12, respectively. Postmortem, mandibular jaws were dissected and cut into blocks around the implants. The explanted tissue blocks were fixed in 10% neutral buffered formalin for 48 h. The tissue blocks were trimmed (Exakt 300 Band System, Exakt, Heraeus Kulzer, Wehrheim, Germany) and dehydrated by ethanol gradient. The blocks were then embedded in methyl methacrylate (Technovit 7200, Exakt). Undecalcified sections were prepared in the buccolingual direction at the central line (Exakt Apparatebau AG, Norderstedt, Germany). Each section was ground and polished to a final thickness (~50 μm) (Isomet 2000, Buehler, Lake Bluff, IL, USA). Two sections were collected from each block. One section was stained with Sanderson and Van Gieson (DHM, Villa Park, IL, USA), and the other section was left unstained for calcein monitoring. Stained (n = 64) and unstained calcein-labeled samples (n = 64) were mounted on glass slides and subjected to histologic evaluations using a microscope (Olympus BX-51, Olympus Optical Co., Tokyo, Japan) connected with video camera and interface card (Olympus DP72, Olympus Optical Co.).

2.5 | Histomorphometric analysis

The regions of interest (ROI) used in this study were 6.0 mm long by 0.35 mm deep segments that corresponded to the external threads or highly porous TM midsections of the implants. Within the ROI segments, the areas occupied by the metallic dental implants were subtracted to calculate the amount of new bone. All histomorphometric analyses were performed using Bioquant Osteo II image analysis software (OsteoMetrics, Inc., Atlanta, GA, USA) interfaced with an Olympus light/epifluorescent microscope and video subsystem.

2.6 | Trabecular bone microarchitecture analysis

Histomorphometric measurements of trabecular bone microarchitecture in the ROI on 64 stained (Sanderson and Van Gieson) slides were performed on an image analyzer (Bioquant Osteo II, OsteoMetrics, Inc.) according to Parfitt's system (Dempster et al., 2013) (Table 1).

2.7 | Chemical and topographical analysis

Scanning electron microscopy (SEM) was employed to visualize and qualitatively analyze the surface morphology or topography of the microtextured titanium surface and the micro- and nano-textured (Bencharit et al., 2014) tantalum surface of the TSV and TM implants, respectively. To determine the surface chemistries of the implants, a scanning electron microscope (Model 6460LV, JEOL USA, Inc., Peabody, MA, USA) with energy-dispersive X-ray spectroscopy

TABLE 1 Histomorphometric measurements of trabecular bone microarchitecture[c]

Symbol	Parameter	Metric	Description
B.Ar	Total new bone area	mm^2	Volume of bone in the ROI[a]
B.Pm	Total new bone perimeter	mcm	Amount of bone surface in the ROI[b]
BS/BV	Bone surface to bone volume	mm^2/mm^3	Ratio of segmented bone surface to the segmented bone volume
T.Ar	Tissue area	mm^2	Volume of bone tissue
Tb.N	Trabecular number	1/mm	Density of trabeculae measured by the number of trabecular plates per unit distance
Tb.Sp	Trabecular separation	mm	Distance between trabeculae
Tb.Th	Trabecular thickness	μm	Width of trabeculae

ROI, region of interest.
[a]two-dimensional measurement.
[b]linear measurement.
[c]Kulak & Dempster, 2010; Dempster et al., 2013; Salamanna et al., 2013.

(EDS) attachment was used to perform qualitative/semiquantitative analyses. Surface mapping microscopy (SMM) using white light interference was conducted with a 3D surface profilometer and optical interferometer (MicroXAM X-100, KLA Tencor Corporation, Milpitas, CA, USA) to measure surface roughness parameters. One TM and one TSV implant were randomly selected for analysis. Areas measuring 129 μm × 172 μm were scanned in 15 locations on each of the two implant surfaces: The trabecular-structured biomaterial was scanned on the TM implant, and the microtextured cervical region was scanned on the TSV implant. All scans were analyzed for the following roughness parameters: absolute mean height deviation (Sa), which is the arithmetic average of the absolute values of the peaks and valleys in the designated measurement region, and root-mean-square surface roughness (Sq), which is the square root of the means of the peaks and valleys in the designated scan area.

2.8 | Statistical analysis

ANOVA general linear model (GLM) (SAS software, version 9.2, SAS, Cary, NC, USA) was used to compare the effects of healing time in histomorphometric data, followed by a post hoc Tukey test. Paired *t* test was used to evaluate the effect of implant types at the same healing times. The level of significance was set at $p < .05$.

3 | RESULTS

3.1 | Dynamic and static histologic evaluations

Both TM and TSV groups showed progressive new bone formation from immature woven bone and bone marrow at 2 weeks to a combination of woven bone and denser lamellar bone with organized fibers at 12 weeks (Figures 2 and 3). Calcein fluorochrome labeling (green) of all unstained histologic sections illustrated the dynamic deposition of mineralized bone matrix at the interface and external perimeter of the implants (Figure 2). Fluorescence was intensely evident at TM implant interfaces and sparse in the TSV interfaces (Figure 2).

3.2 | Histomorphometric data: calcein-labeled histologic slides

Paired t test revealed significant differences in the bone labeling intensity ($p = .045$, .028, and .002 at weeks 2, 8, and 12, respectively) between TM and TSV groups at 2, 8, and 12 weeks, but not at week 4 ($p = .081$) (Figure 4). General linear model (GLM) ANOVA showed no significant differences in the bone labeling intensity for test group ($p > .05$) and control group ($p > .05$), respectively, with respect to healing time.

3.3 | Histomorphometric data: stained histologic slides

Significantly more newly formed bone was observed in the TM group than in the TSV group (paired *t* test, $p = .0014$, .0084, .0218, and .0251 at weeks 2, 4, 8, and 12, respectively) (Figure 5), and GLM ANOVA revealed that the amount of newly formed bone was statistically higher at week 12 than at weeks 2 and 4 ($p = .0138$ in week 2 vs. 12, $p = .0007$ in week 4 vs. 12). In the TSV group, a statistically greater amount of new interfacial bone was observed at the threads with increased healing time ($p = .0373$ in week 2 vs. 8, $p = .0185$ in week 4 vs. 8, $p = .0000$ in week 2 vs. 12, $p = .0000$ in week 4 vs. 12, $p = .0045$ in week 8 vs. 12), except for the comparison between weeks 2 and 4 ($p = .9933$).

3.4 | Histomorphometric data: trabecular bone microarchitecture

Results are summarized in Table 2. The paired t test revealed significant differences ($p = .002$, .026, .005, and .000) in mean specific bone

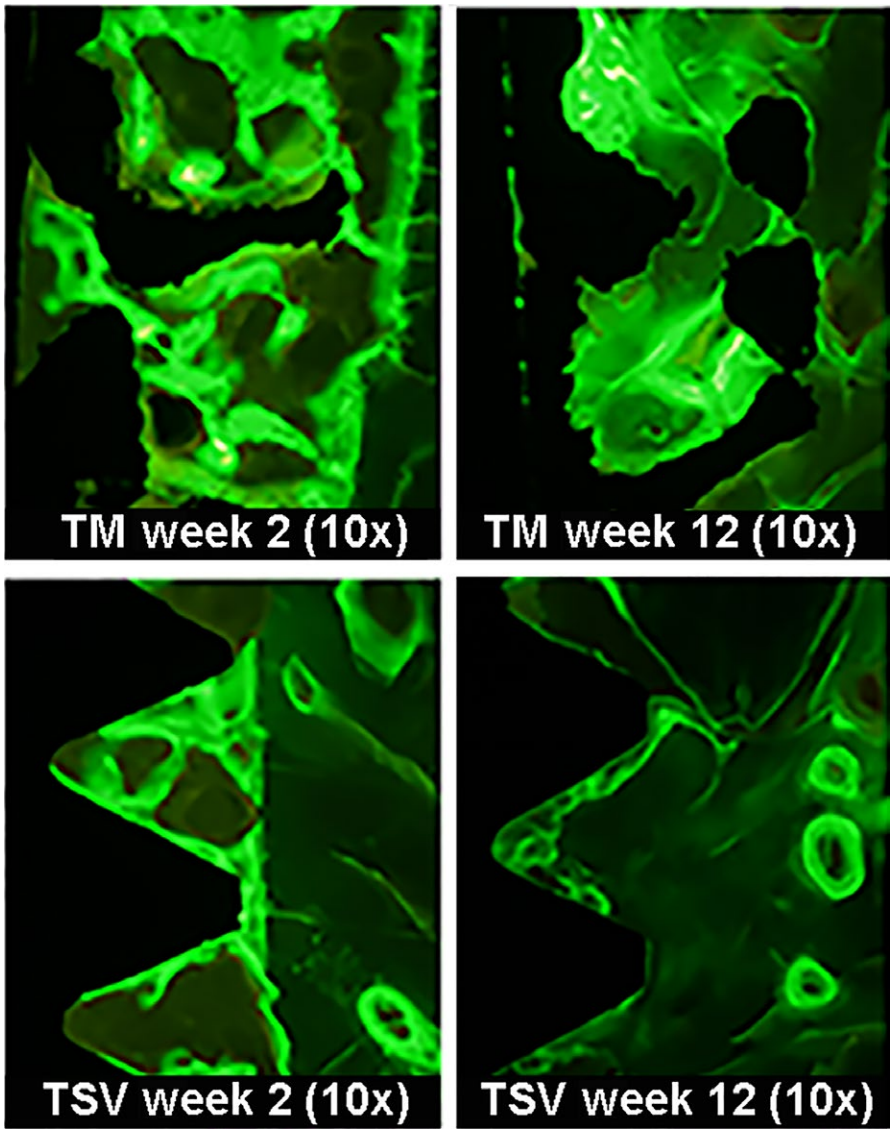

FIGURE 2 Representative calcein-labeled images show greater mineralized bone (green) deposition for TM (top row) compared to TSV (bottom row) implants (black) from 2 (left) to 12 (right) weeks (10× magnification)

surface area values in a given volume between TM and TSV groups at each healing time interval, and that specific bone surface areas increased over time. Mean values of trabecular number were greater (p = .000 and p = .015) for the TM group than for the TSV group at 2 and 4 weeks, respectively. Mean trabecular number values at 2 or 4 weeks were significantly higher for TM group than TSV group, whereas no significant differences were seen in TM group over healing time. At every time interval, the TM group showed significantly higher (p = .010, .023, .004, and .000) mean trabecular thickness values than the TSV group. Mean trabecular separation values were higher (p = .005) in the TSV group than in TM group and increased over time in the TSV group.

3.5 | Chemical and topographical analysis

Representative SEM images of the implant surfaces taken at 500× and 2,000× magnifications are shown in Figure 6. The TM surface exhibits a faceted, granular morphology as compared to the more uniform, microtextured topography of the TSV surface. These differences are related to the CVD and grit-blasting processes that were used to treat the TM and TSV implant surfaces, respectively. The elemental chemical spectra obtained from SEM EDS analysis and 3D mapping of the implant surfaces are shown in Figure 7. The TM surface only showed peaks associated with tantalum, whereas the TSV surface showed peaks associated with the titanium (Ti), aluminum (Al), and vanadium (V) constituents of the titanium alloy (Ti-6Al-4V), as well as calcium (Ca), phosphorus (P), and oxygen (O) peaks associated with grit-blasting the implant surface with HA particles. Sa values of 2.37 μm (±0.53 μm *SD*) and 0.97 μm (±0.08 μm *SD*), and Sq values of 3.02 μm (±0.0.64 μm *SD*) and 1.28 μm (±0.12 μm *SD*) were found for the TM and TSV surfaces, respectively. SMM analysis showed that the TM surface was nearly 150% rougher than the TSV surface.

4 | DISCUSSION

The present study showed that the dynamics of early bone tissue healing in immediately placed implants can be significantly

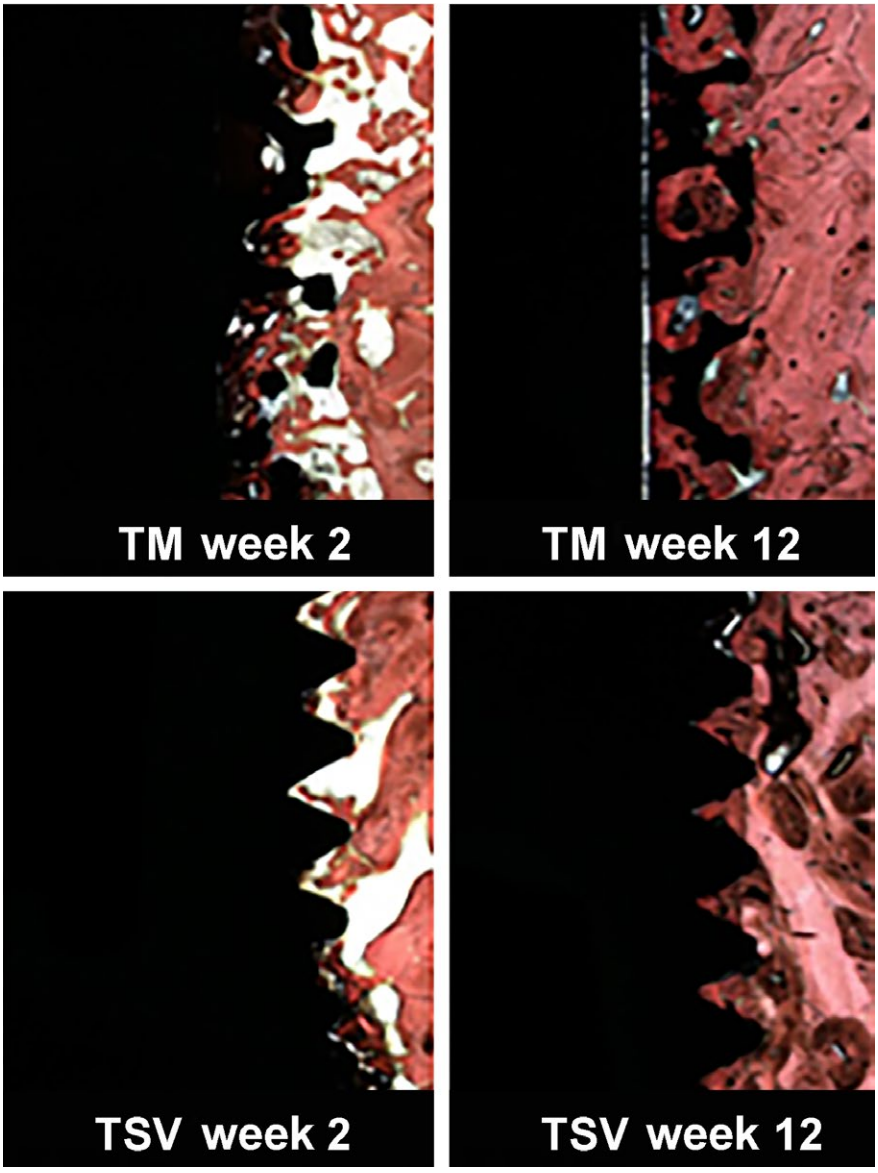

FIGURE 3 Representative histologic images for TM (top row) and TSV (bottom row) implants (black) show progressive bone response (red) from 2 (left) to 12 (right) weeks (Sanderson and Van Gieson stain; 2× magnification)

influenced by implant design. Despite the challenges of immediate implant placement in the canine models, the TM group exhibited faster and more abundant interfacial bone deposition, new bone formation, and remodeling activities than the TSV group (Figures 2-5) (Table 2). The histologic analysis with calcein fluorescent markers (Figure 2) revealed that newly mineralized bone tissues were already present and remodeled as early as 2 weeks postimplantation, which was also clearly evident in the static histologic images with Sanderson and Van Gieson staining (Figure 3). This finding of mineralized and remodeled bone tissue at 2 weeks was consistent with samples retrieved from human subjects by Arriba et al. (2017). Nonetheless, a question has been raised as to whether the use of highly porous TM material in a dental implant design might pose an additional risk for peri-implantitis compared to non-porous implant designs (Bencharit et al., 2014). This is based, in part, on reports in the literature that bacterial adhesion, subgingival bacterial load, and the progression of untreated peri-implantitis are more pronounced on implants with moderately roughened surfaces than implants with smoother surfaces (Berglundh, Gotfredsen, Zitzmann, Lang & Lindhe, 2007; Todescan, Lavigne & Kelekis-Cholakis, 2007).

According to the manufacturer, it is for this reason that use of TM has been restricted to the midsection of the implant approximately 4.25 mm below the prosthetic platform. Consequently, any dental implant with peri-implantitis and 4.0 mm of crestal bone loss would have to be removed whether or not TM material was present if clinical interventions could not alleviate the infection and regenerate the lost bone. In a comparative canine study of ligature-induced peri-implantitis around TM and TSV dental implants, histopathological and histomorphometric findings showed that both implant designs performed similarly and that no bacteria were found inside the pores of the TM material (Battula et al., 2015). In an unrelated case report, a TM implant placed in a patient with moderate chronic periodontitis exhibited peri-implant inflammation affecting one-third of the implant at the second-stage surgical uncovering 4 months after placement (Spinato et al., 2014). The implant was retrieved, and

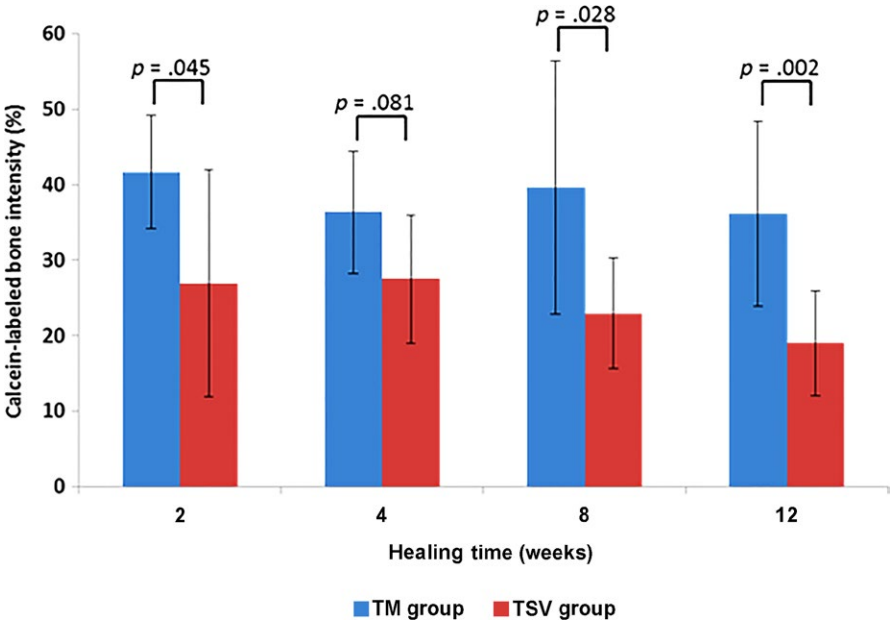

FIGURE 4 Comparison of histomorphometric data from calcein-labeled TM and TSV histologic slides show significant differences in bone labeling intensity at weeks 2 (p = .045), 8 (p = .028), and 12 (p = .002), respectively, but not at week 4 (p = .081)

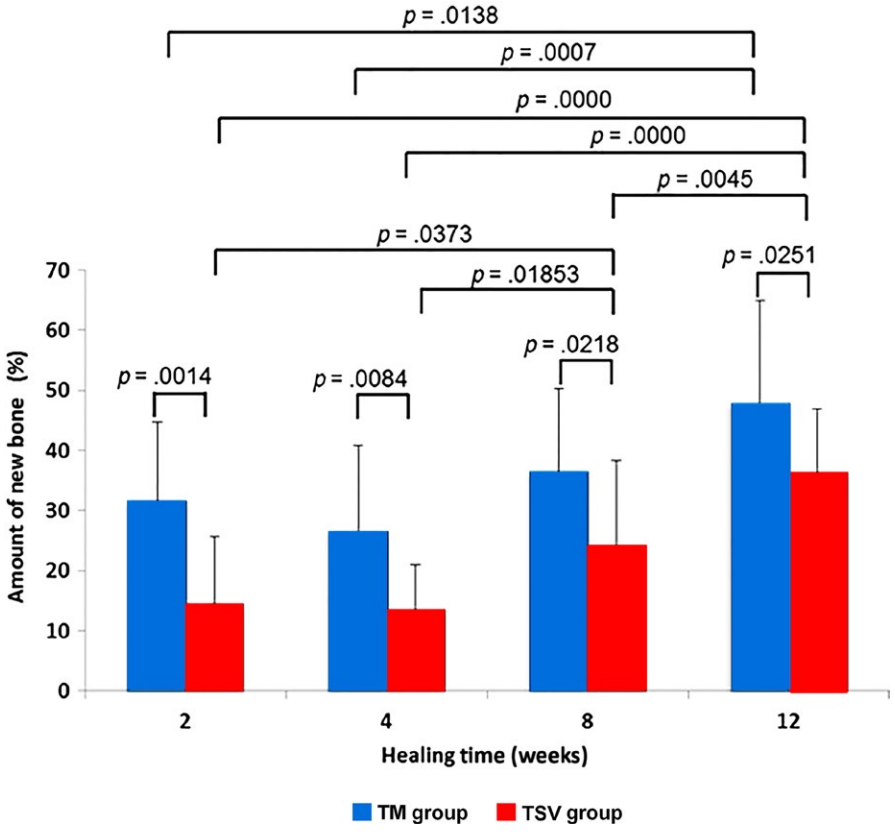

FIGURE 5 Statistical differences in the amount of new bone formation were observed in the TM group compared to the TSV group (p = .0014, .0084, .0218, and .0251 at weeks 2, 4, 8, and 12, respectively) (Sanderson and Van Gieson stains)

histologic analysis found a greater percentage of bone integrated with the tantalum-based TM material than with the implant's titanium surface (Spinato et al., 2014). The authors concluded that TM material promoted bone ingrowth for secondary implant stability and suggested that it may also possess a capacity to resist peri-implant inflammation (Spinato et al., 2014). Although other research has suggested that bacterial adhesion rates are relatively similar between tantalum and titanium (Levon et al., 2010; Schildhauer, Robie, Muhr & Köller, 2006), progressive angiogenesis has been observed (Arriba et al., 2017) inside TM material retrieved from human subjects from 2 to 12 weeks, which may provide a pathway for delivering antibiotics to the internal network of pores inside TM material. Prospective clinical studies are needed, however, before any definitive conclusions can be reached.

TABLE 2 Histomorphometric evaluation of trabecular bone microarchitecture

	Test group	Control group	Between groups
1. Specific bone surface ((BS/BV), unit: mm^2/mm^3)			
Week 2	45.62 ± 13.62	76.21 ± 24.25	p = .002
Week 4	43.79 ± 14.17	62.85 ± 22.76	p = .026
Week 8	33.61 ± 9.17	46.38 ± 10.80	p = .005
Week 12	24.35 ± 5.82	35.62 ± 10.70	p = .000
Over healing time	p = .9670 in week 2 vs. 4	p = .1743 in week 2 vs. 4	
	p = .0186 in week 2 vs. 8	p = .0001 in week 2 vs. 8	
	p = .0604 in week 4 vs. 8	p = .0633 in week 4 vs. 8	
	p = .0000 in week 2 vs. 12	p = .0000 in week 2 vs. 12	
	p = .0001 in week 4 vs. 12	p = .0005 in week 4 vs. 12	
	p = .1022 in week 8 vs. 12	p = .3517 in week 8 vs. 12	
2. Trabecular number ((Tb.N), unit:1/mm)			
Week 2	3.58 ± 1.08	2.07 ± 0.89	p = .000
Week 4	2.67 ± 0.98	1.74 ± 0.76	p = .015
Week 8	3.24 ± 1.00	2.57 ± 0.61	p = .056
Week 12	3.23 ± 1.15	3.06 ± 0.46	p = .582
Over healing time	p = .0827 in week 2 vs. 4	p = .5508 in week 2 vs. 4	
	p = .8107 in week 2 vs. 8	p = .1939 in week 2 vs. 8	
	p = .4210 in week 4 vs. 8	p = .0077 in week 4 vs. 8	
	p = .7934 in week 2 vs. 12	p = .0011 in week 2 vs. 12	
	p = .4402 in week 4 vs. 12	p = .0000 in week 4 vs. 12	
	p = 1.0000 in week 8 vs. 12	p = .2115 in week 8 vs. 12	
3. Trabecular thickness ((Tb.Th), unit: μm)			
Week 2	48.24 ± 16.11	30.10 ± 13.64	p = .010
Week 4	50.05 ± 15.03	35.79 ± 12.70	p = .023
Week 8	63.60 ± 16.92	45.44 ± 10.82	p = .004
Week 12	86.02 ± 17.93	59.67 ± 13.34	p = .000
Over healing time	p = .9896 in week 2 vs. 4	p = .5853 in week 2 vs. 4	
	p = .0520 in week 2 vs. 8	p = .0060 in week 2 vs. 8	
	p = .1054 in week 4 vs. 8	p = .1479 in week 4 vs. 8	
	p = .0000 in week 2 vs. 12	p = .0000 in week 2 vs. 12	
	p = .0000 in week 4 vs. 12	p = .0000 in week 4 vs. 12	
	p = .0017 in week 8 vs. 12	p = .0123 in week 8 vs. 12	
4. Trabecular separation ((Tb.Sp), unit: μm)			
Week 2	261.64 ± 118.99	578.47 ± 354.01	p = .005
Week 4	381.02 ± 185.79	745.63 ± 670.62	p = .051
Week 8	279.72 ± 138.61	364.60 ± 99.15	p = .074
Week 12	265.85 ± 136.43	275.20 ± 58.02	p = .809
Over healing time	p = .1104 in week 2 vs. 4	p = .6087 in week 2 vs. 4	
	p = .9854 in week 2 vs. 8	p = .3991 in week 2 vs. 8	
	p = .2192 in week 4 vs. 8	p = .0329 in week 4 vs. 8	
	p = .9998 in week 2 vs. 12	p = .1251 in week 2 vs. 12	
	p = .1308 in week 4 vs. 12	p = .0052 in week 4 vs. 12	
	p = .9933 in week 8 vs. 12	p = .9119 in week 8 vs. 12	

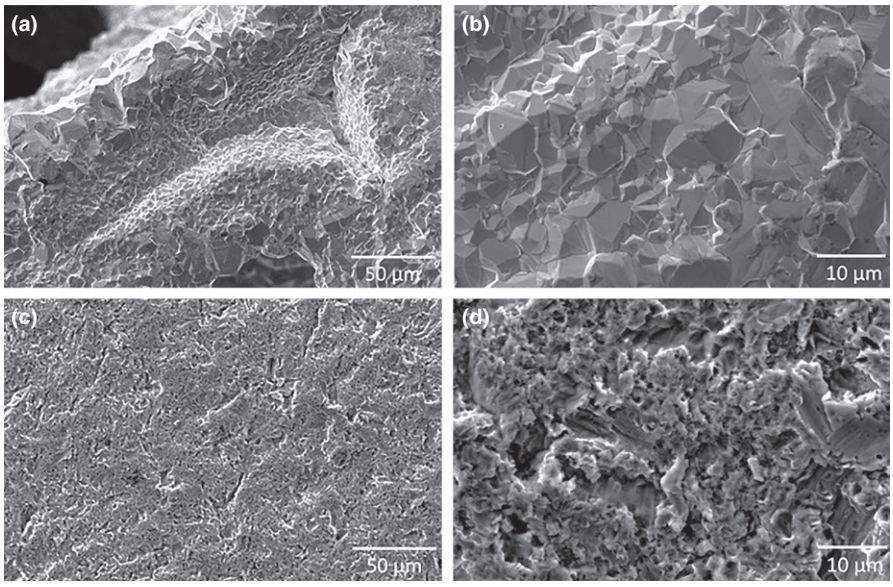

FIGURE 6 SEM enlargements taken at 500× (left) and 2,000× (right) of the TM (a, b) and TSV (c, d) surfaces, respectively. Note the irregular faceted tantalum surface texture (top row) compared to the relatively uniform microtextured titanium surface (bottom row) caused by the CVD and grit-blasting surface preparation methods, respectively

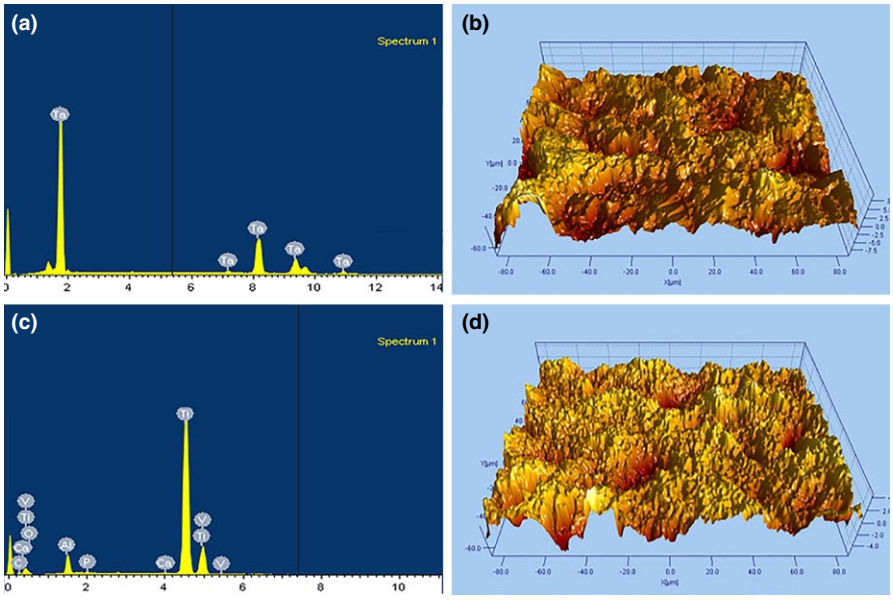

FIGURE 7 Elemental chemical spectra (left) and 3D mapping (right) of the TM (a, b) and TSV (c, d) surfaces, respectively, show significant differences in surface chemistry and roughness parameters

In spite of these findings, it is important to note that the present study had some limitations. First, the sample size of two dogs per time interval was small. An attempt was made to ameliorate this shortcoming by randomly selecting the animals for each healing period, placing the implants in a randomized sequence, and including data from every implant in the study, regardless of the dog, according to the methodology of Kim et al. (2013). Second, the data collected from canine mandibular sites in the present study must be viewed with caution when trying to predict outcomes in humans (Wancket, 2015). While the dog is considered the most preferred large animal species prior to human clinical study in dental implantology, it is true that biological healing rate and immunologic response are different between the two species (Pearce, Richards, Milz, Schneider & Pearce, 2007). Third, all implants were evaluated after unloaded healing in dog mandibles, which characteristically have relatively high bone mineral density (Hao, Zhao, Wang, Yu & Zou, 2014). Therefore, additional research is needed to investigate the effect of loading time on immediate implant placement in the same fresh extraction socket model. Lastly, multiple variables were introduced to the regions of interest between the test and control implant groups, such as implant macrogeometry, surface design/topography, and implant material. These variables may impact the peri-implant healing process differently.

In summary, implant design influences healing dynamics, which can be attributed to the improvement of osseointegration, particularly in situations in that early implant stability is difficult to achieve and maintain. Three-dimensional porosity in the midsection of the TM implant may allow improved mechanical anchorage of the implant by bone ingrowth and neoformation inside the interconnected pores of the biomaterial. Current histologic and histomorphometric

evaluations revealed higher and faster new bone formation in the test group as compared to the control group. Therefore, the TM implant's osseoincorporation model may prove to be a promising alternative to conventional threaded implants and osseointegration alone.

5 | CONCLUSIONS AND CLINICAL IMPLICATIONS

Results suggest that the healing pathway associated with the highly porous midsection of TM dental implant could enable faster and stronger secondary implant stability than conventional osseointegration alone; however, prospective clinical studies are needed to confirm these potential benefits in patients with low bone density, compromised healing, or prior implant failure.

DISCLOSURES

Dr. J.W. Lee, Dr. H.B. Wen, and Dr. P. Gubbi conducted this research while employed by Zimmer Biomet. Dr. G. Romanos has not received any financial support from Zimmer Biomet in connection with this study and does not have any financial interest in any of the products or companies mentioned in this study.

ORCID

Georgios E. Romanos http://orcid.org/0000-0002-7745-5957

REFERENCES

Arriba, C., Gracia, M., Coelho, P. G., Neiva, R., Tarnow, D., Pingarron, M., & Aguado-Henche, S. (2017). *Osseoincorporatin of porous tantalum trabecular-structured metal: A histologic and histomorphometric study in Humans*. The International Journal of Periodontics & Restorative Dentistry,[Epub ahead of print].

Balla, V. K., Bodhak, S., Bose, S., & Bandyopadhyay, A. (2010). Porous tantalum structures for bone implants: Fabrication, mechanical and in vitro biological properties. *Acta Biomaterialia*, *6*, 3349–3359.

Battula, S., Lee, J. W., Wen, H. B., Papanicolaou, S., Collins, M., & Romanos, G. E. (2015). Evaluation of different implant designs in a ligature-induced peri-implantitis model: A canine study. *The International Journal of Oral & Maxillofacial Implants*, *30*, 534–545.

Bencharit, S., Byrd, W. C., Altarawneh, S., Hosseini, B., Leong, A., Reside, G., & Offenbacher, S. (2014). Development and applications of porous tantalum trabecular metal-enhanced titanium dental implants. *Clinical Implant Dentistry & Related Research*, *16*, 817–826.

Berglundh, T., Gotfredsen, K., Zitzmann, N. U., Lang, N. P., & Lindhe, J. (2007). Spontaneous progression of ligature induced peri-implantitis at implants with different surface roughness: An experimental study in dogs. *Clinical Oral Implants Research*, *18*, 655–661.

Bobyn, J. D., Stackpool, G. J., Hacking, S. A., Tanzer, M., & Krygier, J. J. (1999). Characteristics of bone ingrowth and interface mechanics of a new porous tantalum biomaterial. *The Journal of Bone & Joint Surgery British Volume*, *81*, 907–914.

Bobyn, J. D., Toh, K. K., Hacking, S. A., Tanzer, M., & Krygier, J. J. (1999). Tissue response to porous tantalum acetabular cups: A canine model. *Journal of Arthroplasty*, *14*, 347–354.

Dempster, D. W., Compston, J. E., Drezner, M. K., Glorieux, F. H., Kanis, J. A., Malluche, H., & Parfitt, A. M. (2013). Standardized nomenclature, symbols, and units for bone histomorphometry: A 2012 update of the report of the ASBMR Histomorphometry Nomenclature Committee. *Journal of Bone & Mineral Research*, *28*, 2–17.

Deporter, D. A., Watson, P. A., Pilliar, R. M., Chipman, M. L., & Valiquette, N. (1990). A histological comparison in the dog of porous-coated vs. threaded dental implants. *Journal of Dental Research*, *69*, 1138–1145.

Hao, Y., Zhao, W., Wang, Y., Yu, J., & Zou, D. (2014). Assessments of jaw bone density at implant sites using 3D cone-beam computed tomography. *European Review for Medical & Pharmacological Sciences*, *18*, 1398–1403.

Kim, D. J., Huja, S. S., Tee, B. C., Larsen, P. E., Kennedy, K. S., Chien, H. H., & Wen, H. B. (2013). Bone ingrowth and initial stability of titanium and porous tantalum dental implants: A pilot canine study. *Implant Dentistry*, *22*, 399–405.

Kulak, C. A., & Dempster, D. W. (2010). Bone histomorphometry: A concise review for endocrinologists and clinicians. *Arquivos Brasileiros de Endocrinologia & Metabologia*, *54*, 87–98.

Lavenus, S., Louarn, G., & Layrolle, P. (2010). Nanotechnology and dental implants. *International Journal of Biomaterials*, *2010*(915327), 9, https://doi.org/10.1155/2010/915327

Lee, J. W., Wen, H. B., Battula, S., Akella, R., Collins, M., & Romanos, G. E. (2015). Outcome after placement of tantalum porous engineered dental implants in fresh extraction sockets: A canine study. *The International Journal of Oral & Maxillofacial Implants*, *30*, 134–142.

Levon, J., Myllymaa, K., Kouri, V. P., Rautemaa, R., Kinnari, T., Myllymaa, S., & Lppalainen, R. (2010). Patterned macroarray plates in comparison of bacterial adhesion inhibition of tantalum, titanium, and chromium compared with diamond-like carbon. *Journal of Biomedical Materials Research. Part A*, *15*, 1606–1613.

Liu, Y., Bao, C., Wismeijer, D., Hosseini, B., & Wu, G. (2015). The physicochemical/biological properties of porous tantalum and the potential surface modification techniques to improve its clinical application in dental implantology. *Materials Science & Engineering. C, Materials for Biological Applications*, *49*, 323–329.

Pearce, A. I., Richards, R. G., Milz, S., Schneider, E., & Pearce, S. G. (2007). Animal models for implant biomaterial research in bone: A review. *European Cells & Materials*, *13*, 1–10.

Pilliar, R. M. (1998). Overview of surface variability of metallic endosseous dental implants: Textured and porous surface-structured designs. *Implant Dentistry*, *7*, 305–314.

Pilliar, R. M., Cameron, H. U., Binnington, A. G., Szivek, J., & Macnab, I. (1979). Bone ingrowth and stress shielding with a porous surface coated fracture fixation plate. *Journal of Biomedical Materials Research*, *13*, 799–810.

Roldan, J. C., Jepsen, S., Schmidt, C., Knuppel, H., Rueger, D. C., Acil, Y., & Terheyden, H. (2004). Sinus floor augmentation with simultaneous placement of dental implants in the presence of platelet-rich plasma or recombinant human bone morphogenetic protein-7. *Clinical Oral Implants Research*, *15*, 716–723.

Salamanna, F., Fini, M., Parrilli, A., Cadossi, M., Aldini, N. N., Giavaresi, G., & Giannini, S. (2013). Histological, histomorphometric and microtomographic analyses of retrieval hip resurfacing arthroplasty failed at different times. *BMC Musculoskeletal Disorders*, *30*, 14–47. https://doi.org/10.1186/1471-2474-14-47 Retrieved from https://www.ncbi.nlm.nih.gov/pmc/articles/PMC3570284/pdf/1471-2474-14-47.pdf.

Schildhauer, T. A., Robie, B., Muhr, G., & Köller, M. (2006). Bacterial adherence to tantalum versus commonly used orthopedic metallic implant materials. *Journal of Orthopaedic Trauma*, *20*, 476–484.

Schlee, M., Pradies, G., Mehmke, W. U., Beneytout, A., Stamm, M., Meda, R. G., … Bousquet, P. (2015). Prospective, Multicenter Evaluation of Trabecular Metal-Enhanced Titanium Dental Implants Placed in Routine Dental Practices: 1-Year Interim Report From the Development Period

(2010 to 2011). *Clinical Implant Dentistry and Related Research*, *17*, 1141–1153.

Shimko, D. A., Shimko, V. F., Sander, E. A., Dickson, K. F., & Nauman, E. A. (2005). Effect of porosity on the fluid flow characteristics and mechanical properties of tantalum scaffolds. *Journal of Biomedical Materials Research. B, Applied Biomaterials*, *73*, 315–324.

Smith, J. O., Sengers, B. G., Aarvold, A., Tayton, E. R., Dunlop, D. G., & Oreffo, R. O. (2014). Tantalum trabecular metal - addition of human skeletal cells to enhance bone implant interface strength and clinical application. *Journal of Tissue Engineering & Regenerative Medicine*, *8*, 304–313.

Spinato, S., Zaffe, D., Felice, P., Checchi, L., & Wang, H. L. (2014). A trabecular metal implant 4 months after placement: Clinical-histologic case report. *Implant Dentistry*, *23*, 3–7.

Stanford, C. M. (2008). Surface modifications of dental implants. *Australian Dental Journal*, *53*(Suppl 1), S26–S33.

Sun, T. C., Mori, S., Roper, J., Brown, C., & Burr, D. B. (1992). Do different fluorochrome labels give equivalent histomorphometric information? *Bone*, *13*, 443–446.

Todescan, S., Lavigne, S., & Kelekis-Cholakis, A. (2007). Guidance from the maintenance care of dental implants: Clinical review. *Journal (Canadian Dental Association)*, *78*, C107. Retrieved from http://www.jcda.ca/sites/default/files/c107/c107.pdf.

Wancket, L. M. (2015). Animal Models for Evaluation of Bone Implants and Devices: Comparative Bone Structure and Common Model Uses. *Veterinary Pathology*, *52*, 842–850.

Zardiackas, L. D., Parsell, D. E., Dillon, L. D., Mitchell, D. W., Nunnery, L. A., & Poggie, R. (2001). Structure, metallurgy, and mechanical properties of a porous tantalum foam. *Journal of Biomedical Materials Research*, *58*, 180–187.

How to cite this article: Lee JW, Wen HB, Gubbi P, Romanos GE. New bone formation and trabecular bone microarchitecture of highly porous tantalum compared to titanium implant threads: A pilot canine study. *Clin Oral Impl Res*. 2018;29:164–174. https://doi.org/10.1111/clr.13074